ATLAS NOTE

ATLAS-CONF-2010-099

November 23, 2010

Calibrating the b-Tag Efficiency and Mistag Rate of the SV0 b-Tagging Algorithm in 3 pb^{-1} of Data with the ATLAS Detector

The ATLAS collaboration

Abstract

The b-tag efficiency and mistag rate of the ATLAS secondary vertex b-tagging algorithm (SV0) have been measured using data. The b-tag efficiency measurement is based on a sample of jets containing muons and makes use of the transverse momentum of a muon relative to the jet axis ($p_{\mathrm{T}}^{\mathrm{rel}}$). The measurement of the mistag rate is performed on an inclusive jet sample and includes two methods, one which uses the invariant mass spectrum of tracks associated to reconstructed secondary vertices to separate light- and heavy-flavour jets and one which is based on the rate at which secondary vertices with negative decay length significance are present in the data.

Both the b-tag efficiency and mistag rate measured in data depend strongly on the jet kinematics. In the range $25 < p_{\mathrm{T}} < 85$ GeV, the b-tag efficiency rises from 40% to 60%, while the mistag rate increases from 0.2% to 1% between 20 and 150 GeV. The measurements of the b-tag efficiency and mistag rate are provided in the form of p_{T}-dependent scale factors correcting the b-tagging performance in simulation to that observed in data. The b-tag efficiency scale factor is found to be between 0.88 and 1.05 depending on jet p_{T}, with relative uncertainties ranging from 10% to 15%. For light-flavour jets, the simulation underestimates the tag rate by factors of 1.27 ± 0.26 for jets with $p_{\mathrm{T}} < 40$ GeV and 1.07 ± 0.25 for jets with $p_{\mathrm{T}} > 40$ GeV.

1 Introduction

The identification of jets originating from *b*-quarks is an important part of the LHC physics program. In precision measurements in the top quark sector as well as in the search for the Higgs boson and new phenomena, the suppression of background processes containing predominantly light-flavour jets using *b*-tagging is of great use. It is also critical to eventually understand the flavour structure of any new physics (e.g. Supersymmetry) that may be revealed at the LHC.

In order for *b*-tagging to be used in physics analyses the efficiency with which a jet originating from a *b*-quark is tagged by a *b*-tagging algorithm needs to be measured. A second important piece of information is the probability to tag a jet originating from a light-flavour (*u*-, *d*-, *s*-quark or gluon) jet, referred to as the mistag rate. In this note measurements of the *b*-tag efficiency and mistag rate of the SV0 algorithm are presented. The SV0 algorithm is a lifetime-based tagging algorithm which relies on the explicit reconstruction of secondary vertices within jets [1]. The algorithm attempts to reconstruct a single inclusive vertex from all tracks associated to the jet which are displaced from the primary vertex. A jet is considered as tagged if the signed decay length significance, $L/\sigma(L)$, of the reconstructed secondary vertex, computed with respect to the primary vertex, is above a certain value.

The *b*-tag efficiency measurement presented in this note is based on a sample of jets containing muons. The momentum of a muon transverse to the jet axis ($p_{\mathrm{T}}^{\mathrm{rel}}$) is used to obtain the fraction of *b*-jets before and after *b*-tagging.

The measurement of the mistag rate is performed on an inclusive jet sample and is based on two methods. The first method uses the mass distribution of reconstructed secondary vertices, together with knowledge about the *b*- and *c*-tag efficiencies, to determine the fraction of light-flavour jets before and after tagging and hence the mistag rate. The second method counts the rate at which secondary vertices with negative decay length significance are present in the data and then applies corrections, based on simulation, to translate this negative tag rate into a measurement of the mistag rate.

The calibration results are presented as scale factors defined as the ratio of the *b*-tag efficiency or mistag rate in data and simulation:

$$\kappa_{\varepsilon_b}^{\mathrm{data/sim}} = \frac{\varepsilon_b^{\mathrm{data}}}{\varepsilon_b^{\mathrm{sim}}}, \qquad \kappa_{\varepsilon_l}^{\mathrm{data/sim}} = \frac{\varepsilon_l^{\mathrm{data}}}{\varepsilon_l^{\mathrm{sim}}} \tag{1}$$

The *b*-tag efficiency and mistag rate depend not only on the kinematic variables studied in these analyses (jet transverse momentum p_{T} and pseudorapidity η) but also on other quantities such as the fraction of jets in the sample originating from gluons. An advantage of providing the calibration results in the form of scale factors is that even though samples with different event topologies can have slightly different *b*-tag efficiencies or mistag rates, the data-to-simulation scale factors are likely to be valid.

Currently, there is no explicit measurement of the *c*-tag efficiency available in ATLAS. As both the *b*- and *c*-tag efficiencies are dominated by decays of long-lived heavy flavour hadrons, they are expected to show a similar behaviour. In the following it is thus assumed that the scale factor defined in Eq. 1 is the same for *b*- and *c*-jets. However, to take into account any possible deviations from this assumption the systematic uncertainty for the *c*-tag efficiency scale factor is inflated by a factor of two which is considered to be a conservative choice based on simulation studies. In the future, the *c*-tag efficiency will be measured by using dedicated analyses.

This note is organized as follows: Section 2 contains the data sample and object selection used for the measurements, while Section 3 details the samples of simulated events. Section 4 briefly describes the SV0 *b*-tagging algorithm used for the analyses in this note. In Section 5, the measurement of the *b*-tag efficiency is presented, followed by the description of the mistag rate measurement in Section 6. Section 7 summarises the results.

2 Data Sample and Object Selection

The data sample used in the analyses corresponds to approximately 2.9 pb^{-1} of 7 TeV proton-proton collision data collected by the ATLAS experiment between March 30th and August 30th, 2010. For the *b*-tag efficiency measurement, events were collected with a trigger that requires a muon reconstructed from hits in the muon spectrometer which is spatially matched to a calorimeter jet with transverse energy exceeding 5 GeV. The mistag rate measurements use events collected with a logical OR of all jet triggers. In both analyses, only data for which the inner detector, the calorimeters and the muon system pass certain data quality criteria are used. The selected primary vertex [2] has to contain at least ten tracks to ensure good primary vertex resolution.

The key objects used when measuring the *b*-tagging performance are calorimeter jets, inner detector tracks and muons, where the latter two are associated to the calorimeter jets with a spatial matching in $\Delta R(\text{jet}, \text{track}/\mu)$ [3]. Inner detector tracks are required to pass the selection criteria used in the SV0 *b*-tagging algorithm. The muons are reconstructed using information from both the muon system and the inner detector [4]. Muons are required to have $p_{\text{T}} > 4$ GeV and to satisfy the SV0 track selection criteria.

Jets are reconstructed from topological clusters [5] of energy in the calorimeter using the anti-k_t algorithm with a distance parameter of 0.4 [6]. The jet reconstruction is done at the electromagnetic scale and then a scale factor is applied in order to obtain the jet energy at the hadronic scale. The measurement of the jet energy, the current status of the jet energy scale determination and specific cuts used to reject jets of bad quality are described in [7, 8]. The jets used in the *b*-tag efficiency (mistag rate) analysis are required to have $p_{\text{T}} > 25$ GeV ($p_{\text{T}} > 20$ GeV) and $|\eta| < 2.5$. Since the method used to measure the *b*-tag efficiency does not work well for high p_{T} jets (see Section 5 for details), the jets in the *b*-tag efficiency analysis are also required to have $p_{\text{T}} < 85$ GeV.

3 Simulated Samples

The simulated samples used in this measurement are QCD jet samples generated with PYTHIA 6.4.21 [9], utilizing the ATLAS MC09 PYTHIA tune [10], which employs the MRST LO* parton density functions [11] and the p_{T}-ordered parton shower. The simulation has been carried out in seven slices of $\hat{p}_{\perp}$, the momentum of the hard scatter process perpendicular to the beam line [9], starting from $\hat{p}_{\perp} > 8$ GeV. About 1.4 million events have been simulated per $\hat{p}_{\perp}$ slice. To simulate the detector response, the generated events are processed through a GEANT4 [12] simulation of the ATLAS Detector, and then reconstructed and analyzed in the same way as the data [13]. The simulated geometry corresponds to a perfectly aligned detector and the majority of the disabled pixel modules and front-end chips seen in data were masked in the simulation.

The *b*-tag efficiency analysis also makes use of a muon-filtered QCD sample, referred to as the QCD μ-jet sample, which is required to have a muon with $p_{\text{T}} > 3$ GeV at generator level. This sample thus contains muons from *b*- and *c*-decays, but has too few muons from in-flight decays as pions and kaons are treated as stable particles at the generator level. Also for this sample, the simulation has been carried out in slices of $\hat{p}_{\perp}$ with $\hat{p}_{\perp} > 17$ GeV and between 200,000 and 500,000 events in each of the four $\hat{p}_{\perp}$ slices.

To bring the simulation into agreement with data for distributions where discrepancies are known to be present, the following corrections have been applied. The interaction region in *z* is considerably wider in simulation than in data [14]. To correct for this, the distribution of the primary vertex *z* position is reweighted in simulation to follow that observed in data. In addition, the p_{T} spectrum of jets is harder in data than in simulation. Since the *b*-tag efficiency and mistag rate depend strongly on the jet kinematics, the jet p_{T} spectrum in simulation is reweighted to agree with that observed in data.

The labeling of the flavour of a jet in simulation is done by spatially matching the jet with generator level partons: if a b-quark is found within $\Delta R < 0.3$ of the jet direction, the jet is labeled as a b-jet. If no b-quark is found the procedure is repeated for c-quarks and τ-leptons. A jet for which no such association could be made is labeled as a light-flavour jet.

4 The SV0 b-tagging Algorithm

Jets originating from b-quarks are selected by exploiting the long lifetime of b-hadrons (about 1.5 ps) which leads to typical flight paths of a few millimeters which are observable in the detector. The SV0 b-tagging algorithm used in the analyses presented in this note explicitly reconstructs a displaced vertex from the decay products of the long-lived b-hadron. As input, the SV0 tagging algorithm is given a list of tracks associated to the calorimeter jet. Only tracks fulfilling certain quality criteria are used in the secondary vertex fit. Secondary vertices are reconstructed in an inclusive way starting from two-track vertices which are merged into a common vertex. Tracks giving large χ^2 contributions are then iteratively removed until the reconstructed vertex fulfils certain quality criteria. Two-track vertices at a radius consistent with the radius of one of the three Pixel detector layers are removed, as these vertices likely originate from material interactions. A detailed description of the SV0 algorithm can be found in [1].

A jet is considered b-tagged if it contains a secondary vertex, reconstructed with the SV0 tagging algorithm, with $L/\sigma(L) > 5.72$, an operating point that yields a 50% b-tag efficiency in simulated $t\bar{t}$ events. The sign of $L/\sigma(L)$ is given by the sign of the projection of the decay length vector on the jet axis. The $L/\sigma(L)$ distribution in simulation using the QCD jet sample described in Section 3 for b-, c- and light-flavour jets is shown in Fig. 1.

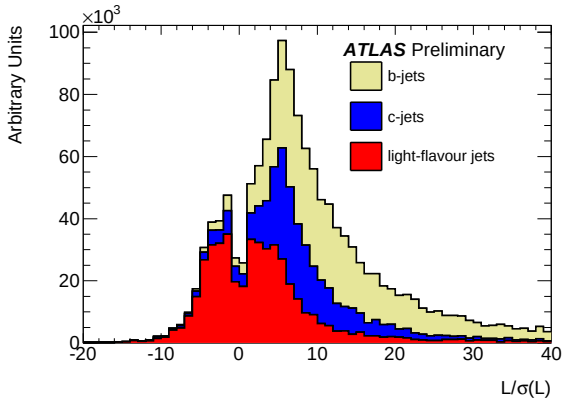

Figure 1: The signed decay length significance $L/\sigma(L)$ for the SV0 b-tagging algorithm in simulation. The distribution extends to much larger values for jets originating from b-quarks compared to those originating from c-quarks, light-flavour quarks or gluons.

5 Measuring the b-tag Efficiency

The b-tag efficiency is defined as the fraction of reconstructed jets originating from b-quarks that are tagged by the SV0 algorithm. In order to extract this quantity from data, the number of b-jets before and after tagging needs to be known. This can be obtained for a subset of all b-jets, namely those containing a muon, using $p_{\mathrm{T}}^{\mathrm{rel}}$ which is defined as the momentum of the muon transverse to the combined muon

plus jet axis. Muons originating from b-hadron decays have a harder $p_{\mathrm{T}}^{\mathrm{rel}}$ spectrum than muons in c- and light-flavour jets. Templates of $p_{\mathrm{T}}^{\mathrm{rel}}$ are constructed for b-, c- and light-flavour jets separately, and these are fit to the $p_{\mathrm{T}}^{\mathrm{rel}}$ spectrum of muons in jets in data to obtain the fraction of b-jets in the pretagged and tagged data samples. The fit is done by adjusting the relative contributions of the b-, c- and light-flavour templates such that the sum of them best describes the $p_{\mathrm{T}}^{\mathrm{rel}}$ shape in data. The pretagged sample is fit using templates derived from all jets passing the jet selection criteria defined in Section 2, while the b-tagged sample is fit using templates derived from jets tagged by the SV0 algorithm. Having obtained the flavour composition of jets containing muons from the $p_{\mathrm{T}}^{\mathrm{rel}}$ fits, the b-tag efficiency is defined as

$$\varepsilon_b^{\mathrm{data}} = \frac{f_b^{\mathrm{tag}} \cdot N^{\mathrm{tag}}}{f_b \cdot N} \cdot C \tag{2}$$

where f_b and f_b^{tag} are the fractions of b-jets in the pretagged and tagged samples of jets containing muons, and N and N^{tag} are the total number of jets in those same two samples. The factor C corrects the efficiency for biases introduced through differences between data and simulation in variables directly affecting the $p_{\mathrm{T}}^{\mathrm{rel}}$ templates. These corrections are further discussed in Section 5.1. The efficiency measured for b-jets with a semileptonically decaying b-hadron in data is compared to the efficiency for the same kind of jets in simulated events to compute the data-to-simulation scale factor defined in Eq. 1. As the b-tag efficiency for hadronic b-jets cannot be determined on data with the method described here, the $\kappa_{\varepsilon_b}^{\mathrm{data/sim}}$ derived from semileptonic b-jets is assumed to be valid for all types of b-jets. Systematic uncertainties associated with this assumption are discussed in Section 5.2.4.

The $p_{\mathrm{T}}^{\mathrm{rel}}$ template fits are performed using a binned maximum likelihood technique where each bin is treated as an independent Poisson variable. The likelihood function used does not include a term for statistical fluctuations in the $p_{\mathrm{T}}^{\mathrm{rel}}$ templates. Instead a systematic uncertainty is assigned to account for the finite template statistics. To avoid including bins with very large statistical fluctuations in the $p_{\mathrm{T}}^{\mathrm{rel}}$ fits, the templates are only derived for $p_{\mathrm{T}}^{\mathrm{rel}} < 2.5$ GeV.

The heavy-flavour content in the sample of jets on which the b-tag efficiency measurement is performed is increased by requiring at least one jet in each event to have a reconstructed secondary vertex with $L/\sigma(L) > 1$, as this reduces the dependence on the modelling of muons in light-flavour jets. For this requirement not to translate into a bias in the analysis, this loosely b-tagged jet, if it contains a muon, is not included in the $p_{\mathrm{T}}^{\mathrm{rel}}$ distributions and thus not used in the efficiency measurement. This flavour-enhancement requirement is not enforced in the sample used to derive the $p_{\mathrm{T}}^{\mathrm{rel}}$ template for light-flavour jets.

The $p_{\mathrm{T}}^{\mathrm{rel}}$ templates for b- and c-jets are derived from the simulated QCD μ-jet sample, using muons associated to b- and c-jets. The templates for light-flavour jets are derived either from data or from the simulated QCD jet sample. The data-derived template is built from all tracks in jets passing the track selection criteria defined in Section 2, with the additional requirement that the p_{T} must exceed 4 GeV, to match the requirement applied to muons. A corresponding track-based template is also derived from tracks in light-flavour jets in simulation. A third light-flavour template comes from muons in light-flavour jets in the simulation. The templates are compared in Fig. 2. All three light-flavour templates were considered in the final measurement, as discussed in Section 5.1.

The $p_{\mathrm{T}}^{\mathrm{rel}}$ method works well for jets with relatively low p_{T}, but becomes unreliable above approximately 85 GeV as these jets become very collimated, and the muon track becomes almost collinear with the jet axis. Due to the finite resolution of the jet direction measurement the $p_{\mathrm{T}}^{\mathrm{rel}}$ distributions for b-, c- and light-flavour jets all become dominated by resolution effects and start to look very similar. It is therefore not possible to tell a b-jet from a non-b-jet based on the $p_{\mathrm{T}}^{\mathrm{rel}}$ of the muon and the method breaks down.

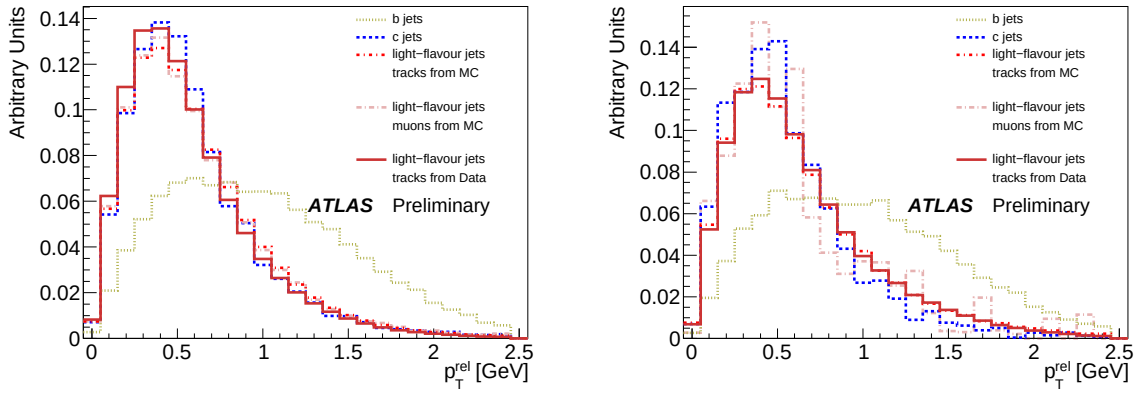

Figure 2: The $p_{\mathrm{T}}^{\mathrm{rel}}$ templates for b-, c- and light-flavour jets, before (left) and after (right) applying a b-tagging requirement. The muons originating from b-hadron decays have a harder $p_{\mathrm{T}}^{\mathrm{rel}}$ spectrum than those in c- and light-flavour jets. The b- and c-templates are derived from muons in jets in the simulated QCD μ-jet sample. The three light-flavour templates shown are derived from muons in light-flavour jets in the simulated QCD jet sample, tracks in light-flavour jets in the simulated QCD jet sample and tracks in jets in data.

5.1 Measurement in Data

As the b-tagging performance depends strongly on the jet momentum and rapidity, the $p_{\mathrm{T}}^{\mathrm{rel}}$ fits are performed in bins of jet p_{T} and jet η. The p_{T} bins used are 25 GeV $< p_{\mathrm{T}} <$ 40 GeV, 40 GeV $< p_{\mathrm{T}} <$ 60 GeV and 60 GeV $< p_{\mathrm{T}} <$ 85 GeV, while the η bins are $0.0 < |\eta| < 1.0$, $1.0 < |\eta| < 1.5$, $1.5 < |\eta| < 2.0$ and $2.0 < |\eta| < 2.5$. Different combinations of templates were used to fit the $p_{\mathrm{T}}^{\mathrm{rel}}$ distribution in data. The sensitivity of the result to the shape of the light-flavour template was investigated by carrying out the fits either with light-flavour templates derived from muons in light-flavour jets in simulation or from tracks in jets in either simulation or data. In addition to varying the light-flavour template, the fits were also repeated omitting either the c- or light-flavour template. This is motivated by the fact that the c- and light-flavour templates look very similar leading to instabilities in the fitted c- and light-flavour fractions. The approach chosen here is more conservative compared to an approach where the ratio of the c- and light-flavour fractions are fixed in the fit to some value estimated e.g. from simulation. As the b-fraction, which is the only fitted quantity that enters the b-tag efficiency calculation, is rather unaffected by changing the non-b model, the maximum difference in b-tag efficiency observed from varying the non-b-templates is only 13%. For the final result, the average of the lowest and highest efficiencies is used, with a systematic uncertainty covering the observed spread. Examples of fits with a b- and a light-flavour template to the $p_{\mathrm{T}}^{\mathrm{rel}}$ distribution in data, before and after tagging, are shown in Fig. 3.

For reasons connected to limited statistics in the simulated QCD μ-jet sample, the p_{T} distribution of the partons emerging from the hard-scatter process is biased. As this sample is used to derive the b- and c-templates, this introduces biases in the $p_{\mathrm{T}}^{\mathrm{rel}}$ template shapes. This bias has been corrected for, and the full change in efficiency due to this correction is taken as a systematic uncertainty. A second correction to the measured b-tag efficiency originates from the modelling in simulation of the b-hadron direction by the calorimeter jet axis. A difference in the jet direction resolution between data and simulation, or e.g. an improper modelling of the angle between the b-quark and the b-hadron in simulation would cause the $p_{\mathrm{T}}^{\mathrm{rel}}$ spectra in simulation and data to disagree, introducing a bias in the measurement. To study this effect, an independent jet axis was formed by vectorially adding the momenta of all tracks in the jet.

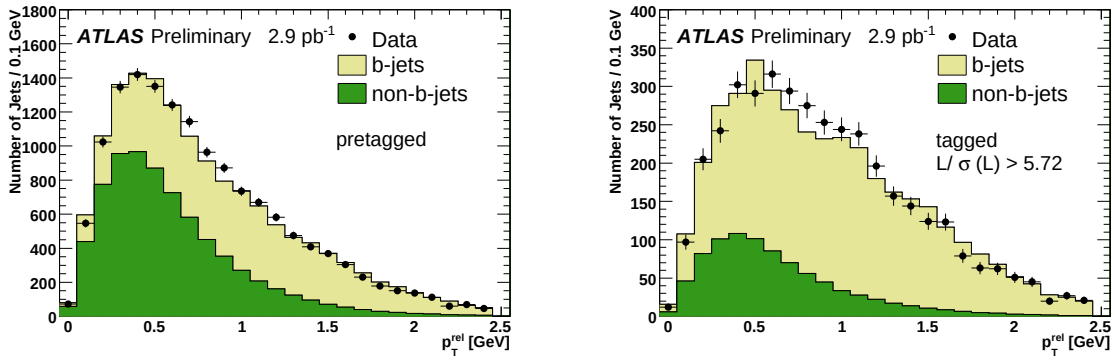

Figure 3: The results of template fits to the $p_{\mathrm{T}}^{\mathrm{rel}}$ distribution in data before (left) and after (right) b-tagging. The fits shown here are performed on jets with p_{T} between 40 and 60 GeV, using two templates (b- and light-flavour jets). Uncertainties shown are for data statistics only. The apparent discrepancies between the data and the sum of the templates are fully covered by the systematic uncertainties on the template shapes.

The difference between this track-based and the standard calorimeter-based jet axis, $\Delta R(\mathrm{calo},\mathrm{track})$, was derived in both data and simulation. In jets which have a reconstructed secondary vertex, an alternate jet axis was also formed from the direction of the vector between the primary and secondary vertices, and this difference, $\Delta R(\mathrm{calo},\mathrm{vtx})$, was compared between data and simulation. There is a slight shift observed between data and simulation in both of these variables. The polar and azimuth angles θ and ϕ of the calorimeter-based jet axis in simulation were therefore smeared such that the $\Delta R(\mathrm{calo},\mathrm{track})$ and the $\Delta R(\mathrm{calo},\mathrm{vtx})$ distributions agreed better with those from data. Smearing based on a Gaussian distribution with a width of 0.015 radians was found to give good agreement between data and simulation. The $p_{\mathrm{T}}^{\mathrm{rel}}$ templates for b- and c-jets were rederived from this smeared sample, and the $p_{\mathrm{T}}^{\mathrm{rel}}$ distribution in data was fit using these altered templates. The efficiency measured in data is corrected for half of the difference in efficiency observed in the unsmeared and the smeared scenarios, and the full difference is taken as a systematic uncertainty. The corrections from the parton p_{T} spectrum and the jet direction yield a factor C (defined in Eq. 2) which ranges from 1.0 for 25 GeV $< p_{\mathrm{T}} <$ 40 GeV to 1.09 for 60 GeV $< p_{\mathrm{T}} <$ 85 GeV.

Figure 4 shows the b-tag efficiency for b-jets containing a muon measured with the $p_{\mathrm{T}}^{\mathrm{rel}}$ method in data, as specified in Eq. 2, together with the true efficiency derived in simulation as a function of the jet p_{T} and η, for a SV0 tag-weight cut of 5.72. The b-tag efficiency measured in data is found to be consistent with that in simulation in all regions of jet η and the efficiency scale factor is therefore only derived in bins of jet p_{T}. The data-to-simulation scale factor as a function of jet p_{T}, after applying the corrections discussed above, is shown in Fig. 5. The scale factor $\kappa_{\varepsilon_b}^{\mathrm{data/sim}}$ is found to be between 0.88 and 1.05, with relative statistical (systematic) uncertainties ranging from 3% to 10% (10% to 12%). As the measurement is only performed for jets with $p_{\mathrm{T}} <$ 85 GeV, the scale factor at larger jet p_{T} is assumed to be that measured in the last p_{T} bin, but with the systematic uncertainty increased by a factor of two.

5.2 Systematic Uncertainties

The systematic uncertainties affecting the $p_{\mathrm{T}}^{\mathrm{rel}}$ method are mainly those that change the shapes of the $p_{\mathrm{T}}^{\mathrm{rel}}$ templates used to fit the sample composition. They can either have a direct impact on $p_{\mathrm{T}}^{\mathrm{rel}}$ or they can indirectly affect the $p_{\mathrm{T}}^{\mathrm{rel}}$ distribution by changing the sample composition or the kinematics of the

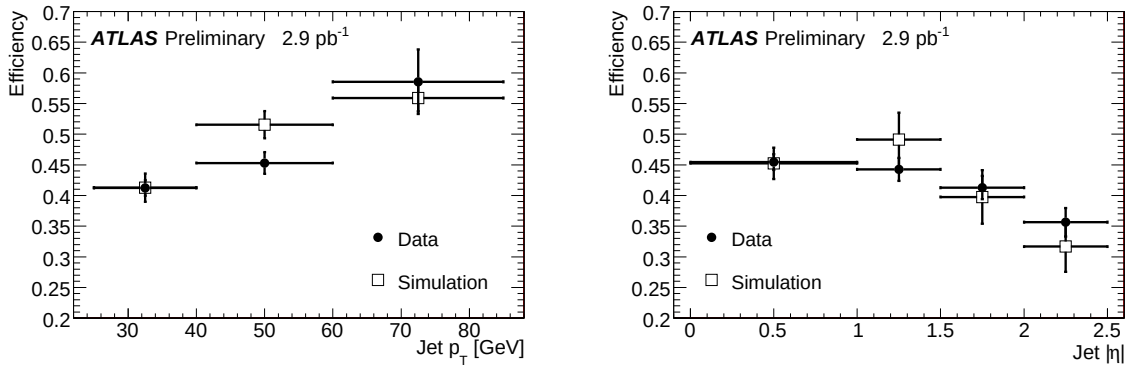

Figure 4: The *b*-tag efficiency for *b*-jets containing a muon in data and simulation as a function of jet p_{T} (left) and jet η (right). Uncertainties are statistical only.

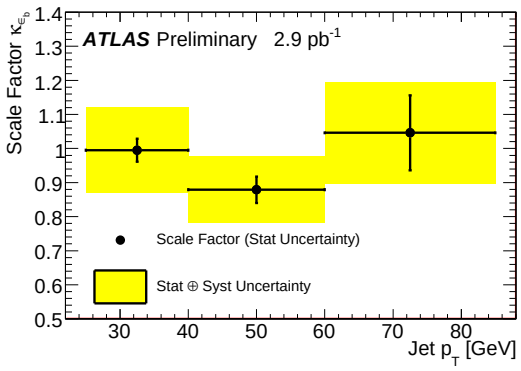

Figure 5: The *b*-tag efficiency scale factor, $\kappa_{\varepsilon_b}^{\mathrm{data/sim}}$, as a function of jet p_{T}. The error bars show the statistical uncertainty while the yellow area shows the total uncertainty (statistical and systematic uncertainties added in quadrature).

sample.

The systematic uncertainties which change the $p_{\mathrm{T}}^{\mathrm{rel}}$ templates are estimated by repeating the $p_{\mathrm{T}}^{\mathrm{rel}}$ fits on data with the modified templates. The exception is the systematic uncertainty originating from limited statistics when building the $p_{\mathrm{T}}^{\mathrm{rel}}$ templates, which is estimated using pseudo-experiments. When estimating systematic uncertainties, the $p_{\mathrm{T}}^{\mathrm{rel}}$ fits performed with the light-flavour template derived from tracks in jets in data are used as the baseline.

The systematic uncertainties are summarized in Table 1. The largest ones arise from the modelling of the *b*-hadron direction, the non-*b*-jet templates and the jet p_{T} spectrum in simulation. The total relative systematic uncertainty is approximately 10%.

Source	Relative Uncertainty		
	$25 < p_{\mathrm{T}}^{\mathrm{jet}} < 40$ GeV	$40 < p_{\mathrm{T}}^{\mathrm{jet}} < 60$ GeV	$60 < p_{\mathrm{T}}^{\mathrm{jet}} < 85$ GeV
Modelling of the *b*-hadron direction	6%	6%	6%
Non-*b*-jet templates	6%	6%	6%
Jet p_{T} spectrum	6%	3%	3%
Scale factor for inclusive *b*-jets	5%	4%	0.7%
$p_{\mathrm{T}}^{\mathrm{rel}}$ template statistics	2%	2%	2%
Modelling of *b*-decays	1.3%	0.2%	0.5%
Fake muons in *b*-jets	0.7%	0.7%	0.7%
Jet energy scale	0.2%	0.2%	0.2%
Modelling of *b*-production	0.2%	0.2%	0.2%
Fragmentation	0.1%	0.1%	0.1%
Total	12%	10%	10%

Table 1: The systematic uncertainties on the efficiency scale factor $\kappa_{\varepsilon_b}^{\mathrm{data/sim}}$. The largest ones arise from the modelling of the *b*-hadron direction, the non-*b*-jet templates and the jet p_{T} spectrum in simulation.

5.2.1 Modelling of the *b*-Hadron Direction

As discussed in Section 5.1, a 100% relative systematic uncertainty is assigned to the correction of the efficiency scale factor due to the difference in the $\Delta R(\mathrm{calo,vtx})$ and $\Delta R(\mathrm{calo,track})$ distributions between data and simulation. This results in a 6% relative systematic uncertainty on the final result.

In principle also the muon direction resolution affects $p_{\mathrm{T}}^{\mathrm{rel}}$, but as the muon angular resolution is very good compared to that of the jet, the uncertainty associated with this is negligible.

5.2.2 Non-*b*-Jet Templates

As discussed in Section 5.1, a systematic uncertainty is assigned to cover the change in the measured *b*-tag efficiency when varying the light-flavour and *c*-templates. This results in a 6% relative systematic uncertainty on the final result.

5.2.3 Jet p_{T} Spectrum

As discussed in Section 5.1, the efficiency measured in data is corrected for the bias introduced by the incorrect p_{T} spectrum of the partons emerging from the hard-scatter process in simulation. The 100% relative uncertainty assigned to this correction results in a 6% relative systematic uncertainty on the

efficiency scale factor in the first jet p_{T} bin and a 3% relative systematic uncertainty in the other two jet p_{T} bins.

5.2.4 Scale Factor for Inclusive *b*-Jets

The $p_{\mathrm{T}}^{\mathrm{rel}}$ method can only measure the *b*-tag efficiency in data for *b*-jets with a semileptonic *b*-hadron decay. As these jets always contain the hard and presumably well-measured muon track, whereas the hadronic *b*-jets do not, the *b*-tag efficiency will be different for these two types of *b*-jets. The ratio in simulation of the *b*-tag efficiency of all *b*-jets to that of *b*-jets with a semileptonic *b*-hadron decay depends on jet p_{T}. It is 60% at low jet p_{T} and approaches one for jets with p_{T} greater than 150 GeV. However, the calibration results in this note are to first order insensitive to this effect as they are given in the form of data-to-simulation scale factors. As long as the simulation models the *b*-tag efficiency in semileptonic and hadronic *b*-jets equally well, the same efficiency scale factor is valid for both types of jets. Therefore, the efficiency scale factor derived as the ratio between the semileptonic *b*-tag efficiency in data and simulation, is assumed to be identical for hadronic *b*-jets.

To investigate the validity of this assumption, the number of tracks, significantly displaced from the primary vertex, in jets with and without muons was compared between data and simulation. The ratio of the normalized track multiplicity distributions for jets without and with muons in simulation was then reweighted to agree with the same ratio in data. The effect on the efficiency in simulation from this reweighting was found to be 5% in the first, 4% in the second and 0.7% in the third jet p_{T} bin, which is taken as a systematic uncertainty on the *b*-tag efficiency scale factor.

5.2.5 $p_{\mathrm{T}}^{\mathrm{rel}}$ Template Statistics

To assess the systematic uncertainty due to the limited statistics available to build the $p_{\mathrm{T}}^{\mathrm{rel}}$ templates, the *b*-, *c*- and light-flavour templates in the pretagged and tagged samples were all varied within their statistical uncertainties, and these pseudo-templates were used to fit the data which was kept fixed. Each pseudo-template was constructed by looping over all bins in the default template histogram and letting each bin content vary around the central value according to a Gaussian distribution with width set to the statistical error in that bin. 10000 pseudo-templates of each kind (*b*, *c*- and light-flavour templates in the pretagged and tagged samples) were constructed, and for each set of pseudo-templates the *b*-tag efficiency was derived from the fit of those templates to the data before and after tagging. The standard deviation of the *b*-tag efficiency distribution of those 10000 pseudo-experiments is taken as the systematic uncertainty. The relative systematic uncertainty arising from this is 2%.

5.2.6 Modelling of *b*-Decays

The muon momentum spectrum in the *b*-hadron restframe, denoted as p^*, directly affects the shape of the $p_{\mathrm{T}}^{\mathrm{rel}}$ distribution for *b*-jets. Uncertainties in the modelling of the p^* spectrum thus have to be taken into account and propagated through the analysis. The p^* spectrum has two components, direct $b \to \mu + X$ decays and cascade $b \to c/\overline{c} \to \mu + X$ decays. Their branching ratios are $BR(b \to lX) = (10.69 \pm 0.22)\%$ and $BR(b \to c/\overline{c} \to lX) = (9.62 \pm 0.53)\%$, respectively [15], giving the ratio $BR(b \to lX)/BR(b \to c/\overline{c} \to lX) = 1.11 \pm 0.065$, where l denotes either a muon or an electron. This ratio of branching ratios has been varied within the quoted uncertainty and the fits have been redone with the modified $p_{\mathrm{T}}^{\mathrm{rel}}$ templates. To investigate the effect of variations of the p^* spectra, a weighting function has been applied to the p^* spectrum of muons from the direct $b \to \mu + X$ decay. This weighting function has been derived by comparing the direct p^* spectrum of $b \to e + X$ decays in PYTHIA as used in the analysis with the corresponding spectrum measured in [16]. The resulting uncertainty from both sources described above is 1.3%, 0.2% and 0.5% for the first, second and third p_{T} bin, respectively.

5.2.7 Fake Muons in b-Jets

The $p_{\mathrm{T}}^{\mathrm{rel}}$ templates for b-jets are obtained from the simulated QCD μ-jet sample where a muon with $p_{\mathrm{T}} > 3$ GeV is required at generator level. This filter will suppress b-jets containing a fake muon rather than a muon from the b-decay. The fraction of fake muons in the $p_{\mathrm{T}}^{\mathrm{rel}}$ templates built from these samples is therefore likely to be lower than in data.

To investigate the impact of fake muons on the b-tag efficiency measurement, $p_{\mathrm{T}}^{\mathrm{rel}}$ fits were performed on the simulated QCD jet sample using b-templates with an increased fake muon fraction. Fake muons were defined as those not matched to a truth track from a muon. The fraction of unmatched muons was found to be 5.3%. This fraction was then increased by a factor of three and the rederived $p_{\mathrm{T}}^{\mathrm{rel}}$ templates were used to fit the fraction of b-jets before and after tagging. The effect on the measured b-tag efficiency is 0.7%, which is taken as a systematic uncertainty.

5.2.8 Jet Energy Scale

A jet energy scale in simulation which is different from that in data would bias the p_{T} spectrum of the simulated events used to build the $p_{\mathrm{T}}^{\mathrm{rel}}$ templates.

The systematic uncertainty originating from the jet energy scale is obtained by scaling the p_{T} of each jet in the simulation up and down by one standard deviation, according to the uncertainty of the jet energy scale [17], and redoing $p_{\mathrm{T}}^{\mathrm{rel}}$ fits on data with the modified b- and c-templates. The jet p_{T} reweighting function was not rederived for the scaled samples, which slightly overestimates the effect of the jet p_{T} scaling. The systematic uncertainty from the jet energy scale is found to be 0.2%.

5.2.9 Modelling of b-Production

In data, b-jets can be produced via several mechanisms: flavour creation, flavour excitation and gluon splitting. In the latter case the angle between the two b-quarks can be so small that both of them end up within the same reconstructed jet. Such b-jets, containing two b-quarks, have a larger probability of being b-tagged than those containing just one b-quark. If the ratio of double-b- to single-b-jets is different in data and simulation that would therefore bias the efficiency scale factor measurement.

The systematic uncertainty associated with the b-production is estimated by varying the ratio of double-b-jets to single-b-jets in simulation and seeing how much that changes the b-tag efficiency. Events containing two b-quarks closer than 0.8 in ΔR were either given a weight of zero or a weight of two (effectively removing or doubling the double-b contribution), and the effect from this on the b-tag efficiency was 0.2%, which was taken as a systematic uncertainty.

5.2.10 Fragmentation

An incorrect modelling of the fragmentation in simulation can affect the momentum spectrum of the muons from the b-decays and thus the $p_{\mathrm{T}}^{\mathrm{rel}}$ distribution. To investigate the impact of fragmentation on the efficiency scale factor, the $p_{\mathrm{T}}^{\mathrm{rel}}$ templates were rederived on a simulated sample where x_b, i.e. the fraction of the b-quark energy carried onto the b-hadron, was changed by 5%. The $p_{\mathrm{T}}^{\mathrm{rel}}$ fits were then redone on data using these altered $p_{\mathrm{T}}^{\mathrm{rel}}$ templates, and the difference in the b-tag efficiency between this and the default scenario was taken as a systematic uncertainty. The impact on the b-tag efficiency from the fragmentation modelling was found to be 0.1%.

5.2.11 Pileup

The instantaneous luminosity has changed by three orders of magnitude during the data taking period used for the b-tag efficiency measurement. Consequently, the level of additional interactions taking place

in the same bunch crossing as the hard-scatter process has increased with time. To understand if the *b*-tagging performance is degraded in the presence of additional pileup vertices, events in data having more than two reconstructed primary vertices were selected, and the efficiency measurement was repeated on this subset. The *b*-tag efficiency was found to not change significantly with respect to the measurement using all data. As a second cross-check, the $p_{\mathrm{T}}^{\mathrm{rel}}$ distribution in data was fit using the light-flavour template from tracks in jets in the pileup-enhanced data sample, and the effect on the *b*-tag efficiency was found to be negligible.

As the efficiency scale factors have been measured on the same dataset as used in physics analyses, any dependence on the *b*-tag efficiency is to first order taken into account. Therefore, pileup was not considered a source of systematic uncertainty in this analysis.

6 Measuring the Mistag Rate

The mistag rate is defined as the fraction of jets originating from light-flavour which are tagged by the SV0 algorithm. Since the mistag rate depends on the kinematics of the jet under consideration, the measurement is performed in bins of jet p_{T} and jet η: 20 GeV $< p_{\mathrm{T}} <$ 40 GeV, 40 GeV $< p_{\mathrm{T}} <$ 60 GeV, 60 GeV $< p_{\mathrm{T}} <$ 90 GeV, 90 GeV $< p_{\mathrm{T}} <$ 140 GeV and 140 GeV $< p_{\mathrm{T}} <$ 200 GeV for jet transverse momentum, $|\eta| < 1.2$ and $1.2 < |\eta| < 2.5$ for the jet pseudorapidity.

The measurement of the mistag rate has been performed by using two independent methods which are described in Sections 6.1 and 6.2. Systematic uncertainties are discussed in Section 6.3 and the combination of the results of the two methods is described in Section 6.4.

6.1 The SV0 Mass Method

This method is based on the determination of the fractions of light-flavour, *c*- and *b*-jets after having applied the SV0 tagging algorithm requiring a reconstructed secondary vertex satisfying $L/\sigma(L) > 5.72$ as defined in Section 1. The discriminating variable chosen to separate light-flavour, *c*- and *b*-jets is the invariant mass of charged particles associated to the inclusively reconstructed secondary vertex, denoted by *SV0 mass* in the following. Templates of the SV0 mass, as derived from simulation, are fit to the SV0 mass distribution from experimental data. Examples of SV0 mass templates and the result of a fit to the data are shown in Fig. 6.

The SV0 mass fits determine the number of *b*-, *c*- and light-flavour jets after applying the tagging requirement (N_b^{tag}, N_c^{tag}, and N_l^{tag}). If the tag efficiencies for *b*- and *c*-jets are known, the number of *b*- and *c*-jets in the pretagged sample can be computed as: $N_b = \frac{N_b^{\mathrm{tag}}}{\varepsilon_b}$ and $N_c = \frac{N_c^{\mathrm{tag}}}{\varepsilon_c}$. The number of light-flavour jets is obtained by subtracting these numbers of *b*- and *c*-jets from the number of all jets before tagging:

$$N_l = N_{data} - N_b - N_c = N_{data} - \frac{N_b^{\mathrm{tag}}}{\varepsilon_b} - \frac{N_c^{\mathrm{tag}}}{\varepsilon_c}. \tag{3}$$

The mistag rate for light-flavour jets is then given by:

$$\varepsilon_l = \frac{N_l^{\mathrm{tag}}}{N_l} = \frac{N_l^{\mathrm{tag}}}{N_{data} - \frac{N_b^{\mathrm{tag}}}{\varepsilon_b} - \frac{N_c^{\mathrm{tag}}}{\varepsilon_c}}. \tag{4}$$

The *b*- and *c*-tag efficiencies in Eq. 4 are taken from simulation, as the measurement in Section 5 shows no large deviations between the efficiencies measured in data and simulation. Systematic uncertainties associated to the *b*- and *c*-tag efficiencies are discussed in Section 6.3.3.

The derivation of the SV0 mass templates from simulation and the determination of the light-flavour mistag rate is performed in bins of jet p_{T} and η as defined in Section 6. The resulting mistag rates are

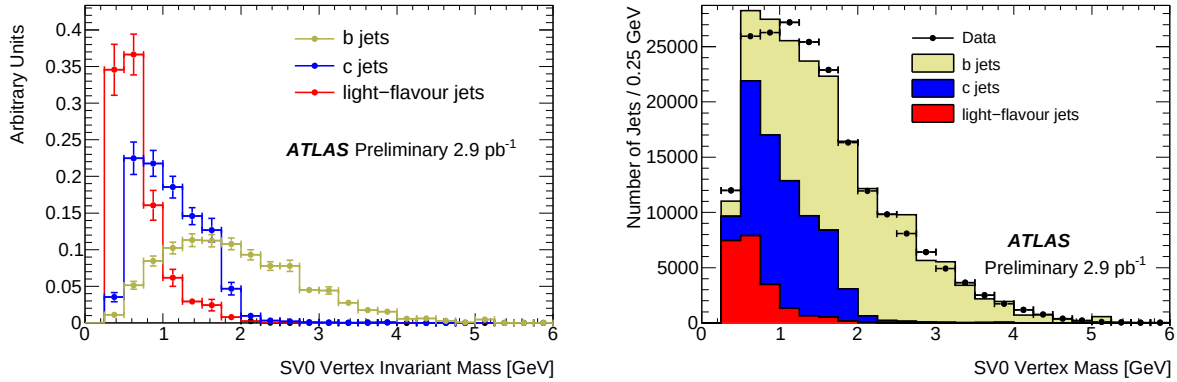

Figure 6: Normalized distributions of SV0 vertex mass fitting templates as used in the SV0 mass method (left) and the result of the fit to experimental data (right). The jets considered in these figures have 40 GeV $< p_{\mathrm{T}} <$ 60 GeV and $|\eta| < 1.2$. In the right plot, uncertainties shown are for data statistics only, and the apparent discrepancies between the data and the sum of the templates are fully covered by the systematic uncertainties on the template shapes.

shown in Fig. 7 and the scale factors $\kappa_{\varepsilon_l}^{\mathrm{data/sim}}$ in Fig. 8. Systematic uncertainties will be discussed in Section 6.3.

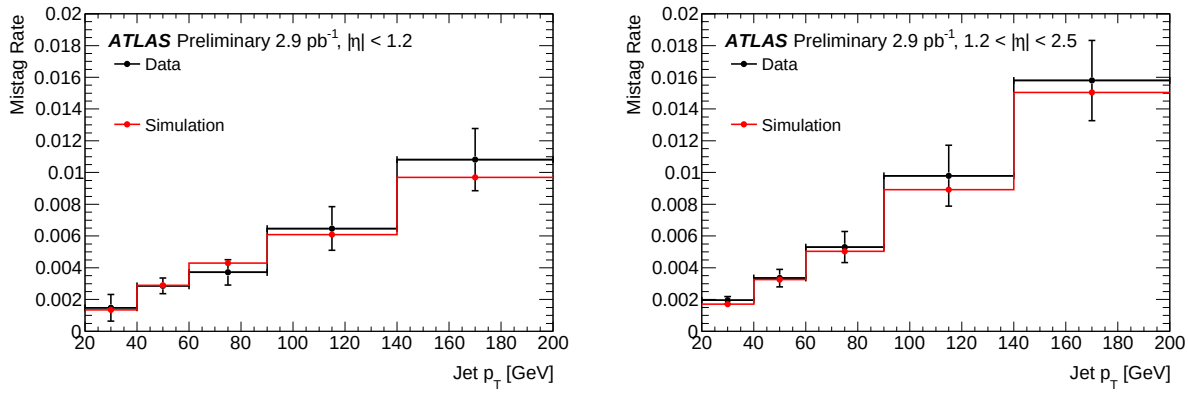

Figure 7: Expected and observed mistag rates for the SV0 mass method for central ($|\eta| < 1.2$; left) and forward jets ($1.2 < |\eta| < 2.5$; right). The plots show the total uncertainties.

6.2 The Negative Tag Method

The method described in this section is based on the use of *negative tags*, where negative tags in the case of the SV0 tagging algorithm studied here means placing the tagging cut at $L/\sigma(L) < -5.72$ instead of $L/\sigma(L) > 5.72$. Light-flavour jets are mistakenly tagged as b-jets mainly because of the finite resolution of the inner detector and the presence of tracks stemming from displaced vertices from long-lived particles or material interactions. The resolution component is expected to give rise to a $L/\sigma(L)$ distribution which is symmetric around zero. The distribution on the negative side can thus be used to determine the light-flavour mistag probability if proper corrections, accounting for the mistags due to long-lived particles and material interactions, are applied. The mistag rate ε_l is approximated by the negative tag rate of

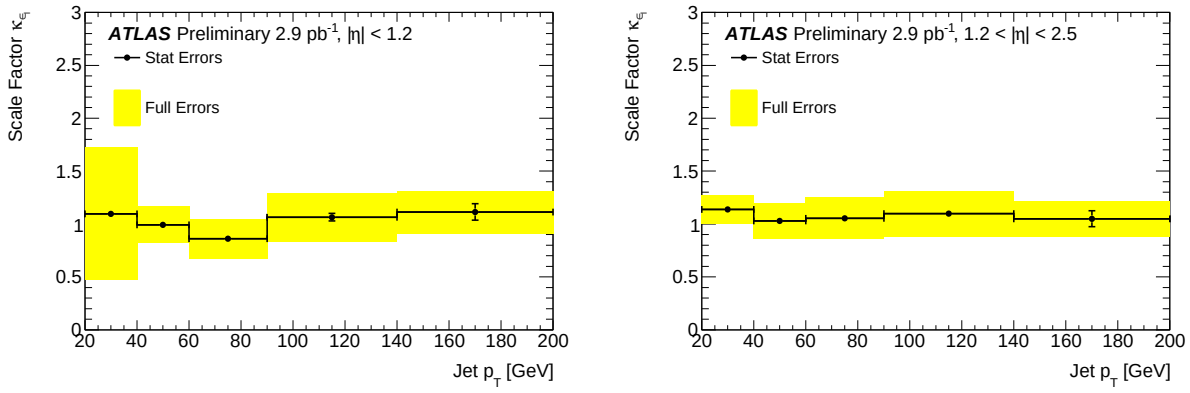

Figure 8: The mistag rate scale factors $\kappa_{\varepsilon_l}^{\mathrm{data/sim}}$ for the SV0 mass method for central ($|\eta| < 1.2$; left) and forward ($1.2 < |\eta| < 2.5$; right) jets.

the inclusive jet sample, ε_{inc}^{neg}. This approximation would be exact if the negative part of the distribution used for the tagging of jets (the decay length significance $L/\sigma(L)$ in case of the SV0 tagging algorithm) looked identical for all jet flavours and the tagging distribution for light-flavour jets was perfectly symmetric around zero. However, since this is not the case, two corrections have to be applied to relate ε_{inc}^{neg} to ε_l:

- The negative tag rate for *b*- and *c*-jets differs from the negative tag rate for light-flavour jets. *b*- and *c*-jets are positively tagged mainly because of the measurable lifetimes of *b*- and *c*-hadron decays, shifting the decay length significance distributions towards larger values. However, effects like the finite jet direction resolution can flip the sign of the discriminating variable, increasing significantly the negative tag rate for *b*- and *c*-jets. The correction factor $k_{hf} = \varepsilon_l^{neg}/\varepsilon_{inc}^{neg}$ is defined to account for this effect. Because of the effects described above and the relatively small fractions of *b*- and *c*-jets in the inclusive sample, k_{hf} is typically smaller than, but close to unity.

- A symmetric decay length significance distribution for light-flavour jets is only expected for fake secondary vertices arising e.g. from track reconstruction resolution effects. However, a significant fraction of reconstructed secondary vertices have their origin in charged particle tracks stemming from long-lived particles (K_s^0, Λ^0 etc.) or material interactions (hadronic interactions and photon conversions). These vertices will show up mainly at positive decay length significances and thus cause an asymmetry for the positive versus negative tag rate for light-flavour jets. The correction factor $k_{ll} = \varepsilon_l/\varepsilon_l^{neg}$ is defined to account for this effect. Because of the sources in light-flavour jets showing positive decay length, k_{ll} is larger than unity.

For the $L/\sigma(L) > 5.72$ operating point calibrated here, the correction factor k_{hf} is very close to one whereas k_{ll} is about 3.5 for central jets and up to 7 for forward jets, with a very small dependence on the jet p_{T}. With these correction factors, which are derived from simulation, the mistag rate is computed from the inclusive negative tag rate:

$$\varepsilon_l = \varepsilon_{inc}^{neg}\, k_{hf}\, k_{ll}\,. \tag{5}$$

The resulting mistag rates are shown in Fig. 9 and the scale factors $\kappa_{\varepsilon_l}^{\mathrm{data/sim}}$ in Fig. 10.

6.3 Systematic Uncertainties

Several sources of systematic uncertainties have been studied, covering both instrumental effects (e.g. tracker performance, material interactions) as well as modelling of the underlying physics processes in

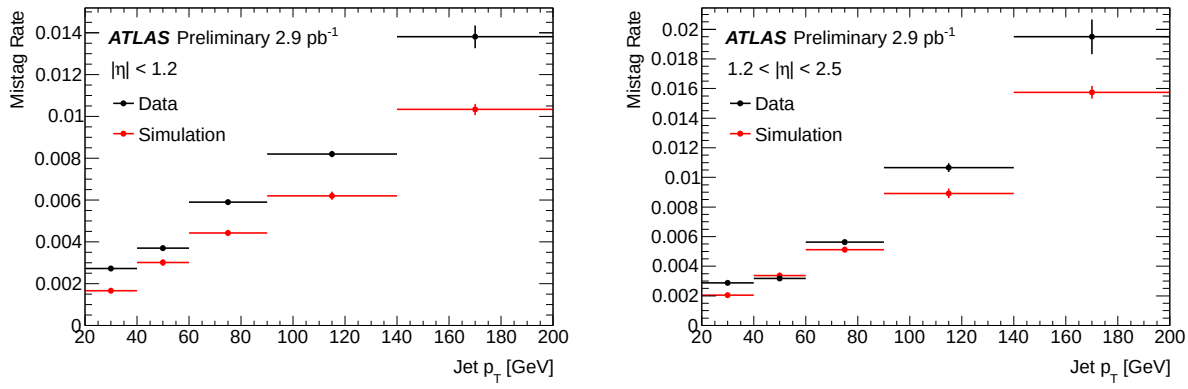

Figure 9: Expected and observed mistag rates for the negative tag method for central ($|\eta| < 1.2$; left) and forward jets ($1.2 < |\eta| < 2.5$; right). The plots show statistical uncertainties only.

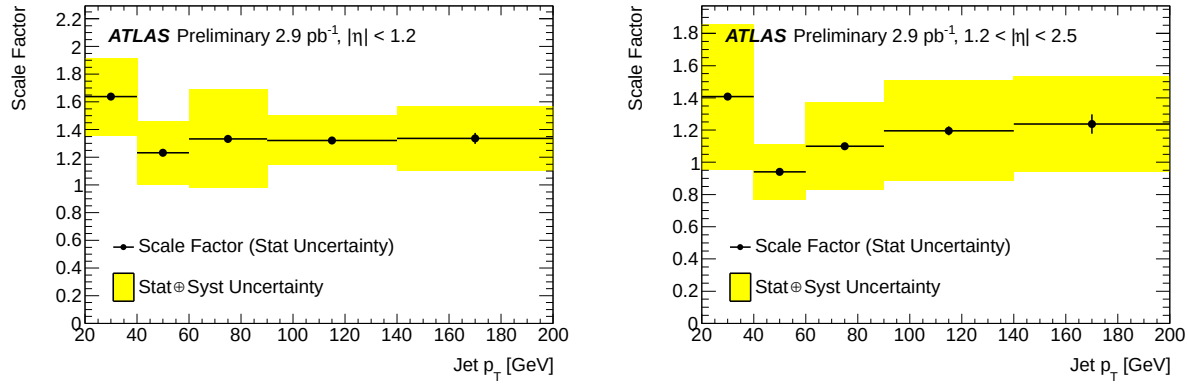

Figure 10: The mistag rate scale factors $\kappa_{\varepsilon_l}^{\mathrm{data/sim}}$ for the negative tag method for central ($|\eta| < 1.2$; left) and forward ($1.2 < |\eta| < 2.5$; right) jets.

the Monte Carlo generator.

Variations of parameters in the simulation related to these sources typically lead to modified shapes of the secondary vertex mass templates (for the SV0 mass method) or modified values for the correction factors k_{hf} and k_{ll} (for the negative tag analysis) which are then propagated through the analyses to derive the systematic uncertainties.

The systematic uncertainties on the mistag rate which have been considered are discussed below.

6.3.1 Jet Energy Scale

A bias in the jet energy measurement in simulation compared to data will result in a distortion of the secondary vertex mass shapes for the SV0 mass method and biases in the correction factors k_{hf} and k_{ll} for the negative tag method if there is a correlation between the jet energy and these quantities. To study this effect, the reconstructed jet energies were alternately shifted up and down by 7% and half of the full difference of the corresponding shifts of the mistag rates were assigned as systematic uncertainty. The resulting uncertainties range up to about 10%.

6.3.2 Run Period Dependence, Trigger Modelling

Both analyses observe a dependence of the scale factor $\kappa_{\varepsilon_l}^{\mathrm{data/sim}}$ on the data taking run period. This effect may be related to biases introduced by the trigger selection (the inclusive jet triggers used in these analyses have undergone substantial changes in the prescale factors applied to them with evolving instantaneous luminosity) which have not been modeled in the selection of simulated events. Additional studies have been performed by repeating the analyses using only subleading jets (the ones that probably did not fire the trigger) and subdividing the data sample in different periods with different trigger configurations. The subdivision in run periods is also sensitive to any dependence of the mistag rate on the level of additional pileup vertices, as the instantaneous luminosity has changed by three orders of magnitude during the data taking period used for the mistag rate measurement. The resulting uncertainties range up to about 20% .

6.3.3 Heavy Flavour Tagging Efficiencies

The tagging efficiencies for *b*- and *c*-jets directly enter into the SV0 mass analysis through Eq. 4 and into the negative tag analysis through the correction factor k_{hf}. The *b*- and *c*-tag efficiencies as obtained from simulation have been varied by 15 (20)% and 30 (40)%, respectively, for the SV0 mass (negative tag) analysis. With these variations the efficiencies are in agreement with the measurement described in Section 5. The uncertainties on the *b*- and *c*-tag efficiencies have been increased for the negative tag analysis compared to the SV0 mass analysis as they include the uncertainty on the extrapolation from the positive tag efficiency (the one measured in data) to the negative one. Since the tag rate of both *b*- and *c*-jets is mainly driven by the real lifetime of *b*- and *c*-hadrons, these uncertainties have been taken to be fully correlated and thus have been varied together. The resulting uncertainties are about 3% and 5% for the SV0 mass and negative tag analyses, respectively.

6.3.4 Heavy Flavour Fractions

The fractions of *b*- and *c*-jets enter directly into the correction factor k_{hf} for the negative tag analysis. Uncertainties on the *b*- and *c*-jet fractions of 10% and 30% have been propagated through the analysis. These uncertainties are motivated by fitting templates of distributions that discriminate between the different flavours, e.g. the invariant mass of tracks significantly displaced from the primary vertex, to the data. The resulting uncertainty is about 2%.

6.3.5 Heavy Flavour Properties

Inaccuracies in the modelling of *b*- and *c*-hadrons can lead to distortions of the mass templates for *b*- and *c*-jets used in the SV0 mass analysis. The most obvious bias would arise from shifted *b*- and *c*-hadron masses. The masses of reconstructed secondary vertices in *b*- and *c*-jets have been shifted by 2%, motivated by studies of the secondary vertex mass distributions in heavy-flavour dominated control regions in data, to account for this effect. The resulting uncertainty ranges up to 10% for the highest jet p_{T} bins.

6.3.6 Simulation Statistics

Large numbers of simulated events are needed to accurately model the vertex mass templates used in the fits to the data for the SV0 mass analysis. To address the uncertainty due to the limited simulation statistics the bin contents of the mass templates have been varied within their statistical uncertainties. For the negative tag analysis, the statistical uncertainties on k_{hf} and k_{ll} have been propagated through the analysis. The resulting uncertainties are about 10%.

6.3.7 Track Multiplicity

The simulation does not properly describe the multiplicity of tracks associated to jets. This could be due to an imperfect modelling of fragmentation, the relative fraction of quark and gluon jets in the light-flavour sample or differences in the track reconstruction in data and simulation (the charged particle multiplicity in *b*-hadron decays is quite accurately known). Reweighting schemes have been applied to match the observed track multiplicity distributions in data and simulation for the inclusive jet sample (for the negative tag analysis) or to shift the track multiplicity distribution for light-flavour jets before applying the *b*-tagging requirement (for the SV0 mass analysis). The resulting uncertainties are typically below 3%.

6.3.8 Long-Lived Particle Decays, Material Interactions, Fake Tracks

The decay products from decays of long-lived particles like e.g. K_s^0, Λ^0, hadronic interactions or photon conversions in the detector material (mainly interactions in the first material layers of the detector) may cause reconstructed secondary vertices in light-flavour jets. While the SV0 algorithm applies a veto to secondary vertices consistent with these decays or interactions, not all of these can be detected and there is a sizable fraction of vertices where one track arising from such decays or interactions is paired with a track from a different source into a vertex. Fake or badly-measured tracks may also give rise to additional vertices. To estimate the resulting systematic uncertainty, the fraction of jets containing long-lived particles like K_s^0 and Λ^0 or material interactions have been varied by 20% and 10%, respectively. These variations are motivated by studies of reconstructing K_s^0 decays, photon conversions and nuclear interactions in the detector material as well as other studies sensitive to material effects (e.g. the K_s^0 mass in data compared to simulation) and comparing results from data and simulation. The rate of badly measured tracks has been estimated based on the χ^2/DOF of the track fit and varied by 30% for the negative tag analysis. The other sources causing a tagging asymmetry in the negative tag analysis have been varied by 20%. The resulting uncertainties are below 2% for the SV0 mass analysis and about 6% for the negative tag analysis.

6.3.9 Track Impact Parameter Resolutions

Inclusive secondary vertex reconstruction is very sensitive to tracking resolutions and proper estimation of the errors, especially in light-flavour jets where a large contribution of fake vertices is present. It

has been shown in [14] that the track impact parameter resolutions in simulation are slightly better than those in data. Therefore, track impact parameters in the simulation have been smeared in order to bring data and simulation into better agreement. The chosen smearing approach does not take into account correlated modifications of the impact parameters of tracks that pass through the same pixel module, as would be needed to model residual misalignments in the inner detector. The parameters for the smearing have been chosen to cover the observed discrepancies in the impact parameter resolution between data and simulation in a conservative way. After having applied the track impact parameter smearing to the tracks in simulation, the primary vertex reconstruction and *b*-tagging have been rerun and the whole analyses repeated. The resulting uncertainties range up to about 15%.

6.4 Combination of Mistag Rate Results

The results from the SV0 mass method (Section 6.1) and the negative tag method (Section 6.2) were combined using the Best Linear Unbiased Estimator (BLUE) method [18]. In the combination, the number of kinematic bins for the mistag scale factor was reduced from ten to two: one for jets with $p_{\mathrm{T}} < 40$ GeV, and another for jets with $p_{\mathrm{T}} > 40$ GeV, where in both p_{T} ranges the two η ranges $|\eta| < 1.2$ and $1.2 < |\eta| < 2.5$ have been combined. For each analysis eight kinematic bins in p_{T} and η are above 40 GeV, so all sixteen of these are treated as separate measurements and combined accordingly. For the low p_{T} combination, however, the measurement in the jet η range $|\eta| < 1.2$ from the SV0 mass measurement has such high uncertainties that it was excluded from the combination and the other three measurements were used.

In the combination, statistical uncertainties in both data and simulation are treated as uncorrelated, while the systematic uncertainties are treated as fully correlated within each individual method. Moreover, most systematic uncertainties are treated as fully correlated between the two methods. The exceptions are the uncertainties on the pretag flavour fractions for the negative tag method, and the heavy flavour modelling uncertainty for the SV0 mass method, which are treated as uncorrelated to any systematic uncertainty from the other analysis. The systematic uncertainty originating from the modelling of the track impact parameter resolutions in simulation is anti-correlated between the two measurements (the smearing of the impact parameter distributions raises the measured mistag rate for the SV0 mass analysis and lowers it for the negative tag analysis). As this is the largest uncertainty in both measurements, the cancellation of this systematic uncertainty in the final result that would occur if this source of uncertainty was treated as fully anti-correlated in the combination, is considered overly aggressive. The combination is thus performed without considering the smearing uncertainty and this systematic uncertainty is instead added in quadrature to the systematic uncertainty obtained in the combination. Uncertainties of 12% and 14% have been taken as conservative estimates for the two jet p_{T} bins. The same approach is taken for the trigger uncertainty where a 16% (19%) uncertainty has been assigned to the first (second) jet p_{T} bin. Table 2 summarises the uncertainties for the combined result, where *Other* denotes all uncertainties, including the statistical one, that have been individually considered with their correlations in the combination.

7 Results

Both the *b*-tag efficiency and mistag rate measured in data depend strongly on the jet kinematics. The calibrations to be used in physics analyses are therefore instead provided in the form of p_{T}-dependent scale factors correcting the *b*-tag efficiency or mistag rate in simulation to that measured in data. The *b*-tag efficiency and mistag rate scale factors, $\kappa_{\varepsilon_b}^{\mathrm{data/sim}}$ and $\kappa_{\varepsilon_l}^{\mathrm{data/sim}}$, are shown in Fig. 11.

For the *b*-tag efficiency, the scale factor is close to one for all values of jet p_{T}. The measured scale

Source	Relative Uncertainty	
	$20 < p_{\mathrm{T}} < 40$ GeV	$p_{\mathrm{T}} > 40$ GeV
Track Impact Parameter Resolutions	12%	14%
Run Dependence, Trigger	16%	19%
Other	7%	4%
Total	21%	24%

Table 2: The systematic uncertainties on the mistag rate scale factor $\kappa_{\varepsilon_l}^{\mathrm{data/sim}}$.

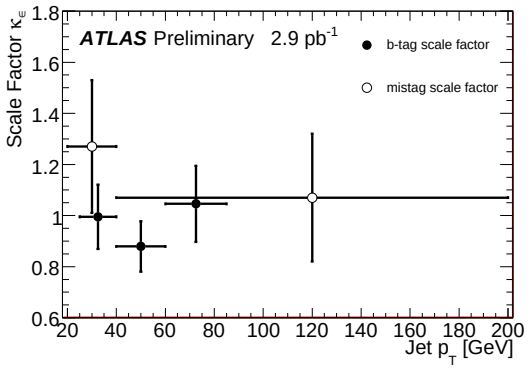

Figure 11: The final scale factors, $\kappa_{\varepsilon_b}^{\mathrm{data/sim}}$ and $\kappa_{\varepsilon_l}^{\mathrm{data/sim}}$, as a function of jet p_{T}. The error bars show the total uncertainty (statistical and systematic uncertainties added in quadrature).

factors are:

$$
\begin{aligned}
25 < p_{\mathrm{T}} < 40\ \mathrm{GeV} &: 1.00 \pm 0.03\ (\mathrm{stat}) \pm 0.12\ (\mathrm{syst}) \\
40 < p_{\mathrm{T}} < 60\ \mathrm{GeV} &: 0.88 \pm 0.04\ (\mathrm{stat}) \pm 0.09\ (\mathrm{syst}) \\
60 < p_{\mathrm{T}} < 85\ \mathrm{GeV} &: 1.05 \pm 0.11\ (\mathrm{stat}) \pm 0.10\ (\mathrm{syst})
\end{aligned}
$$

The largest systematic uncertainties arise from the modelling of the b-hadron direction, the non-b-jet templates and the jet p_{T} spectrum in simulation. The measurement is only made for jets with $p_{\mathrm{T}} < 85$ GeV. For jets with larger p_{T}, the scale factor in the $60 < p_{\mathrm{T}} < 85$ GeV bin is used, but the systematic uncertainty is inflated by a factor of two.

The mistag rate scale factors are obtained by combining the results of the two mistag analyses as described in Section 6.4. The combination yields a mistag scale factor of 1.27 ± 0.26 for jets with $p_{\mathrm{T}} < 40$ GeV and 1.07 ± 0.25 for jets with $p_{\mathrm{T}} > 40$ GeV. The largest systematic uncertainties arise from the smearing of the impact parameter resolution in simulation and from the modelling of the trigger.

As a final validation, the b-tag efficiency and mistag rate scale factors were applied, on a jet-by-jet basis, to the tagged jets in simulation, and the resulting number of tagged jets were compared to an inclusive jet sample in data. The result is shown in Fig. 12, as a function $L/\sigma(L)$. The overall normalization of the simulation was done by scaling the number of pretagged jets in simulation to match the data. As the number of tagged jets does not only depend on the efficiencies and mistag rates but also on the flavour composition of the pretagged sample, the flavour fractions in simulation have been adjusted to those obtained from template fits to the SV0 mass distribution in data. Systematic uncertainties associated with this have not been propagated to the uncertainty on the simulated distribution.

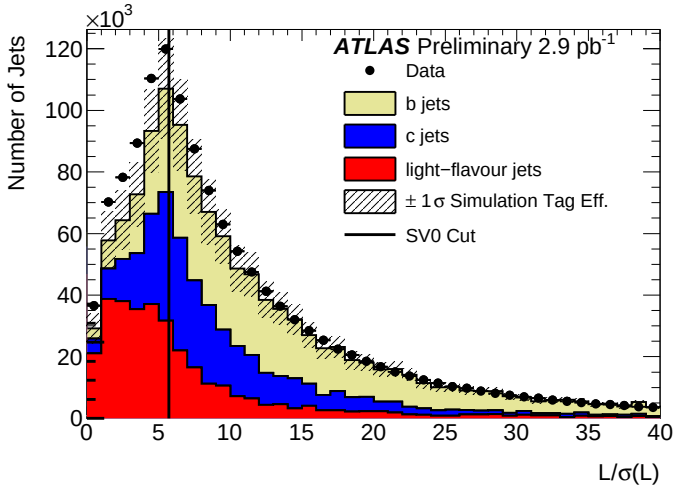

Figure 12: The signed decay length significance $L/\sigma(L)$ for the SV0 b-tagging algorithm in data (points) and simulation (stacked histogram) for an inclusive jet sample. The cut used in the analyses, $L/\sigma(L) > 5.72$, is indicated by the vertical line. The contributions of the different flavours in simulation have been scaled by the b-tag efficiency and mistag rate scale factors as measured in this note. The flavour composition of the pretagged sample is taken from data, however the systematic uncertainties associated with this do not contribute to the uncertainty on the simulated distribution.

8 Conclusions

In this note, measurements of the *b*-tag efficiency and mistag rate of the SV0 tagging algorithm were presented. Jets were considered *b*-tagged if the signed decay length significance of the reconstructed secondary vertex was greater than 5.72 (an operating point that yields a 50% *b*-tag efficiency for jets in simulated $t\bar{t}$ events). Both the *b*-tag efficiency and mistag rate measured in data depend strongly on the jet kinematics. In the range 25 GeV $< p_{\mathrm{T}} <$ 85 GeV, the *b*-tag efficiency rises from 40% to 60%, while the mistag rate increases from 0.2% to 1% between 20 GeV and 150 GeV.

The calibration results are given in the form of p_{T}-dependent scale factors which correct the *b*-tag efficiency or mistag rate in simulation to that measured in data. The *b*-tag efficiency scale factor is found to be between 0.88 and 1.05 depending on jet p_{T}, with relative statistical (systematic) uncertainties ranging from 3% to 10% (10% to 12%). The mistag rate scale factor is found to be 1.27 ± 0.26 for jets with $p_{\mathrm{T}} < 40$ GeV and 1.07 ± 0.25 for jets with $p_{\mathrm{T}} > 40$ GeV.

Currently, there is no explicit measurement of the *c*-tag efficiency available in ATLAS. As both the *b*- and *c*-tag efficiencies are dominated by decays of long-lived hadrons, they are expected to show a similar behaviour. It is therefore assumed that the *b*-tag efficiency scale factor is valid also for *c*-jets. However, to take into account any possible deviations from this assumption, the systematic uncertainty for the *c*-tag efficiency scale factor is inflated by a factor of two.

References

[1] The ATLAS Collaboration, *Performance of the ATLAS Secondary Vertex b-tagging Algorithm in 7 TeV Collision Data*, ATLAS-CONF-2010-042, May, 2010.

[2] G. Piacquadio, K. Prokofiev, and A. Wildauer, *Primary vertex reconstruction in the ATLAS experiment at LHC*, J. Phys. Conf. Ser. **119** (2008) 032033.

[3] The ATLAS Collaboration, *Expected performance of the ATLAS experiment: Detector, Trigger and Physics, Volume 1*, CERN-OPEN-2008-020, December, 2008.

[4] The ATLAS Collaboration, *Muon Performance in Minimum Bias pp Collision Data at* $\sqrt{s} = 7$ *TeV with ATLAS*, ATLAS-CONF-2010-036, June, 2010.

[5] G. Aad et al., *The ATLAS Experiment at the CERN Large Hadron Collider*, JINST **3** (2008) S08003.

[6] M. Cacciari, G. P. Salam, and G. Soyez, *The anti-k(t) jet clustering algorithm*, JHEP **04** (2008) 063.

[7] The ATLAS Collaboration, *Properties of Jets and Inputs to Jet Reconstruction and Calibration with the ATLAS Detector Using Proton-Proton Collisions at sqrt(s)=7 TeV*, ATLAS-CONF-2010-053, June, 2010.

[8] The ATLAS Collaboration, *Data-Quality Requirements and Event Cleaning for Jets and Missing Transverse Energy Reconstruction with the ATLAS Detector in Proton-Proton Collisions at a Center-of-Mass Energy of* $\sqrt{s} = 7$ *TeV*, ATLAS-CONF-2010-038, May, 2010.

[9] T. Sjostrand, S. Mrenna, and P. Z. Skands, *PYTHIA 6.4 Physics and Manual*, JHEP **05** (2006) 026.

[10] The ATLAS Collaboration, *ATLAS Monte Carlo tunes for MC09*, ATL-PHYS-PUB-2010-002, March, 2010.

[11] A. Sherstnev and R. S. Thorne, *Parton Distributions for LO Generators*, Eur. Phys. J. **C55** (2008) 553–575.

[12] GEANT4 Collaboration, S. Agostinelli et al., *GEANT4: A simulation toolkit*, Nucl. Instrum. Meth. **A506** (2003) 250–303.

[13] ATLAS Collaboration, *The ATLAS Simulation Infrastructure*, The European Physical Journal C - Particles and Fields (2010) 1–52. 10.1140/epjc/s10052-010-1429-9.

[14] The ATLAS Collaboration, *Tracking Studies for b-tagging with 7 TeV Collision Data with the ATLAS Detector*, ATLAS-CONF-2010-070, July, 2010.

[15] Particle Data Group Collaboration, K. Nakamura et al., *Review of particle physics*, J. Phys. **G37** (2010) 075021.

[16] BABAR Collaboration, B. Aubert et al., *Measurement of the electron energy spectrum and its moments in inclusive $B \to Xe\nu$ decays*, Phys. Rev. **D69** (2004) 111104.

[17] The ATLAS Collaboration, *ATLAS Calorimeter Response to Single Isolated Hadrons and Estimation of the Calorimeter Jet Scale Uncertainty*, ATLAS-CONF-2010-052, July, 2010.

[18] L. Lyons, D. Gibaut, and P. Clifford, Nucl. Instrum. Meth. A270 (1988) 110; A. Valassi, Nucl. Instrum. Meth. A500 (2003) 391.